Spatio-Temporal Evaluation of Agricultural Drought Indices Using Remote Sensing and Soil Moisture Data in the Shiriya River Basin.

Abha J P, Sreerama Naik S R*, T K Prasad and Jayapal G

Department of Geography, Kannur University, SAT Campus, Payyanur, Kerala.

***Corresponding Author**

DOI: https://doi.org/10.47772/IJRISS.2026.100700867

Received: 29 July 2026; Accepted: 03 August 2026; Published: 14 August 2026

ABSTRACT

The current study presents an exploratory analysis in the Shiriya River Basin of the relationship between agricultural drought and LULC dynamics using remote sensing data over the period from 2002 to 2026. We used multi-sensor time series data to estimate rainfall, land surface temperature, and drought. The analysis was carried out using the NDVI, LST, VCI, SMI, TCI, VHI, and TVDI indicators. Rainfall showed a certain increase (trend line slope = 40.78mm/year; Sen's slope) over the period, although with significant year-to-year variability. The LST was characterised by a slight decrease (trend line slope = -0.0988°C/year; Sen's slope). There were extreme temperature fluctuations, particularly in 2006 and 2018. Based on the vegetation indicator data (NDVI, VCI, VHI), it was found that the study basin was dominated by vegetation with signs of significant improvement for the period 2002–2022; the share of vegetation in the basin was about 27% and increased to 88%.

An increase in the level of soil moisture and a decrease in thermal stress confirmed this trend. SMI, TCI, and TVDI data indicate positive dynamics of the study area and the localised occurrence of drought throughout the period. However, the analysis of the last three years reveals signs of fragmentation of vegetation and significant fluctuations in surface temperature. The LULC data for 2026 indicate a decrease in the share of agricultural land to 18% with the transformation of the forest into barren land, an increase in the specific weight of built-up areas both fragmented and contiguous, and a decrease in the share of fallow land. The analysis showed that the basin has been experiencing improvement during the period under review and has been relatively free of drought. At the same time, these positive trends are gradually being replaced by signs of stress for the period of study in 2026.

Keywords: Agricultural Drought; Soil Moisture Index (SMI); NDVI; Vegetation Health Index (VHI); Temperature Vegetation Dryness Index (TVDI); Remote Sensing.

INTRODUCTION

Climate change is a severe problem faced by humanity today. The warming phase has accelerated the water cycle, and it shows significant and lasting changes in the statistical distribution of extreme weather events such as drought and floods (Dai, 2013). Among natural disasters, drought is considered one of the least understood and most expensive (Kao and Govindaraju, 2010). Droughts are classified into many types, including meteorological, agricultural, hydrological, and socioeconomic droughts (American Meteorological Society, 1997). Among these, agricultural droughts (soil moisture droughts) have a much shorter time scale (McKee et al., 1993) but can still affect human society. Agricultural drought refers to a shortage of soil moisture during the growing season such that crops cannot meet their water needs, leading to reduced growth and yield, even when total annual rainfall may not be exceptionally low (Sreekesh et al., 2019). Remote sensing techniques provide an effective means of monitoring agricultural drought through vegetation- and water related indices, enabling spatial assessment and early warning of drought conditions (Mistry & Suryanarayana, 2023). It links different aspects in space, including climate, soil, plants, and farm management. A large number of drought indices have been proposed, such as VCI, TCI, TVDI, VHI, and SMI. The assessment of agricultural drought requires an integrated approach that considers both climatic parameters and vegetation responses. Remote sensing indices provide a reliable means to capture these dynamics, allowing for spatially explicit drought monitoring and an early warning system.

Soil Moisture Index (SMI) maps relative surface soil wetness. It is commonly computed from combinations of land surface temperature and vegetation indices (Saha et al. al, 2019). SMI is widely used to detect and monitor agricultural drought because it tracks soil water stress that affects crops. It captures soil and surface moisture dynamics that are closely linked to evapotranspiration and crop stress, improving the detection of agricultural drought impacts (Palagiri & Pal, 2023). Both optical thermal methods and microwave-based SMI formulations offer complementary advantages and can be integrated to enhance drought analysis**.** It is valuable for farm-scale to regional drought monitoring and early warning when calibrated against ground observations or fused with microwave products to mitigate cloud and vegetation effects (Wang et al., 2020; Sun et al., 2021).

Normal Difference Vegetation Index (NDVI) is a measure of vegetation vigour and health derived from optical remote sensing data (Kourouma et al., 2021). It is computed using the reflectance in the red and near-infrared bands and is widely used to assess vegetation condition and biomass (Almeida-Ñauñay et al., 2022). It is a dimensionless index; hence, its values range from -1 to +1 (Meneses-Tovar,2011), where higher positive values indicate more vigorous green vegetation and values near zero or negative typically correspond to non-vegetated surfaces, while increasing positive values reflect increasing canopy greenness and biomass (Mayouf & Hanafi, 2024). Declines in NDVI have been used to detect and characterise moisture stress and agricultural drought, and NDVI derivatives have been applied in drought analysis and early warning systems(Chakraborty & Sehgal, 2010). It has practical limitations that can affect interpretation and is routinely transformed into vegetation condition metrics such as the VCI and is integrated with temperature-based components into VHI for improved drought assessment.

Land Surface Temperature (LST) relates directly to how the surface emits thermal radiation and is retrieved from thermal infrared (TIR) satellite brightness temperatures converted to surface temperature estimates (Bento et al., 2018). It is widely used in drought indices such as TCI and TVDI. The TCI is explicitly derived from TIR–derived LST and serves as the thermal component of the VHI alongside the VCI (Canedo-Rosso et al., 2021). It functions as a very important indicator of local climate and vegetation condition because it reflects how every surface divides incoming energy between sensible heat and latent heat fluxes. Changes in LST have been used to infer changes in surface energy balance, soil moisture, and evapotranspiration (Zhang et al., 2021; Dudumashe & Thomas, 2020).

The Vegetation Condition Index (VCI) (Kogan, 1995b) is computed from satellite-derived NDVI and used to represent vegetation condition for each pixel (Sorman et al., 2018). VCI values span from 0 to 100, where lower values indicate severe vegetation stress and higher values represent favourable conditions (Hang et al., 2024). It has been used to detect and map agricultural drought severity and to compare meteorological drought indices and crop yield impacts (Bento et al., 2018; Rahman et al., 2025).

The Temperature Condition Index (TCI) is a satellite-derived metric that quantifies thermal stress on vegetation using thermal infrared observations, a formulation associated with Felix Kogan (Kogan, 1995a); its values span from 0 to 100, where lower values indicate very severe drought and higher values indicate the absence of drought. It is obtained from Land Surface Temperature (LST) and represents the temperature component of vegetation health assessments **(**Bento et al., 2018; Boudjemline & Benlabiod, 2022). Studies applying Landsat data routinely derive TCI from LST to capture heat stress signals independent of green biomass observations (Li et al.,2023; Yu & Guo, 2023). It is merged with the Vegetation Condition Index (VCI) to detect and monitor drought impacts on vegetation. VCI captures vegetation vigour while TCI captures temperature-induced stress. TCI can be sensitive to meteorological drought at seasonal scales in some ecosystems, making it a valuable complement to VCI in multi-index drought assessments (Bento et al., 2020).

The Temperature Vegetation Dryness Index (TVDI) combines LST and NDVI to estimate surface moisture conditions. This index maps each pixel's temperature relative to NDVI-dependent wet and dry edges in the Temperature-NDVI space, so higher TVDI implies drier surface conditions (Liu & Yue, 2018). The LST- NDVI scatter typically forms a triangular or trapezoidal domain where the lower edge represents the wet edge and the upper edge represents the dry edge; alternative bi-parabolic shapes have been reported in low-biomass regions

ISSN No. 2454-6186 | DOI: 10.47772/IJRISS | Volume X Issue VII July 2026

and accounted for in modified TVDI methods. It has been applied for regional and long-term drought assessment and trend analysis across provinces and basins, including comparisons of drought extent and temporal change (Liu & Yue, 2018; Liu et al., 2015). It correlates negatively with soil moisture and precipitation and can capture major drought events, but performance drops in very dense vegetation or very sparse vegetation (Huang et al., 2025).

Vegetation Health Index (VHI) quantifies vegetation condition by jointly accounting for vegetation state and thermal stress. It responds to declines in vegetation signal and to increased thermal stress that suppresses vegetation activity (Serban & Maftei, 2025). VHI combines two components: Vegetation Condition Index from NDVI and Temperature Condition Index from LST (Zeng et al., 2023; Bento et al.,2018). Values of VHI range from 0 to 100; low VHI implies stressed vegetation or drought, and high VHI implies healthy vegetation (Shahzaman et al., 2021; Shoumik et al., 2023). Captures both moisture stress and heat stress, making it more accurate than NDVI or VCI alone for detecting vegetative drought, especially in non-homogeneous and agriculture-dependent regions (Chere et al.,2022).

METHODOLOGY

2.1 Data

This study utilised multi-temporal imagery from the Landsat program to analyse the spatial and temporal variations in agricultural drought conditions. Landsat 7 ETM+, Landsat 8 OLI/TIRS and Landsat 9 OLI-2/TIRS-2 imagery were used for the analysis. Images were selected from a consistent seasonal window (March to May) to minimise seasonal variability and facilitate reliable temporal comparison. Cloud and cloud shadow masking was applied during image processing to minimise atmospheric distractions. The Landsat imagery was used to derive NDVI and LST, from which the vegetation, temperature and moisture-related drought indices were subsequently generated.

Sl. No.	Parameter	Data	Source
1	• NDVI • LST • VCI • TCI • SMI • TVDI • VHI	Landsat 7 ETM+, 8 OLI/TIRS, 9 OLI-2/TIRS-2	USGS /Google Earth Engine
2	• Study Area Extraction	DEM	CartoDEM (ISRO Bhuvan)
3	• LULC	Landsat Imagery	Google Earth Engine
4	• Rainfall	CHIRPS	CHC/Google Earth Engine

Table No. 1: Data used for analysis

Methods

Normalised Difference Vegetation Index (NDVI): This remote sensing metric is used to assess live green vegetation by measuring the contrast between near-infrared (NIR) (strongly reflected by vegetation) and red wavelengths (strongly absorbed). NDVI values range from -1 to 1, with higher values indicating healthier vegetation and lower values indicating barren land, water bodies, or stressed plants.

$$NDVI = (NIR - Red) / (NIR + Red)$$

For the study, NDVI values were classified into (-1.00-0.00) non-vegetated, (0.01-0.30) sparse vegetation, (0.31-0.60) moderate vegetation, and (0.61-1.00) dense vegetation classes (Laksono et al., 2020).

Vegetation Condition Index (VCI): This index helps assess the effect of moisture on vegetation. It ranges from 0% to 100%, with lower values indicating severe drought or poor vegetation and higher values indicating optimal conditions. In 2004, Kogan put forward the following equation to calculate VCI.

VCI= 100 * (NDVI-NDVImin) / (NDVImax-NDVImin)

VCI range is classified into 0-20 (extreme drought), 20-40 (severe drought), 40-60 (moderate drought), 60-80 (light drought) and 80-100 (very light drought) (Vallejo et al., 2019).

Temperature Condition Index (TCI): To overcome the limitations of the VCI under cloud-contaminated conditions, temperature-based indices such as the TCI are used, as they incorporate thermal information for a more reliable drought assessment (Shastri & Mujumdar, 2025). The TCI evaluates the thermal stress on vegetation. Lower values indicate higher temperature stress and possible drought conditions in the region. The value arranged based on 0-20 (very severe drought), 20-40 (severe drought), 40-60 (moderate drought), 60-80 (very low drought) and 80-100 (no drought) (Das et al.,2013).

TCI= 100 * (LSTmax-LST) / (LSTmax-LSTmin)

Land Surface Temperature (LST) was derived from thermal infrared bands to estimate the surface temperature. It is a key parameter for understanding the surface energy balance and drought conditions. LST max is the maximum value of the retrieved LST, and LST min is the minimum value of the retrieved LST. LST was derived from thermal bands to estimate surface temperature. It is a key indicator of surface heating and drought conditions in the region. LST was classified into five thermal categories: very low (≤28°C), low (28–32°C), moderate (32–36°C), high (36–40°C), and very high (≥40°C).

Soil Moisture Index (SMI): The SMI was computed to estimate surface soil moisture conditions. The resulting values range from 0 to 1; higher values indicate wetter conditions, whereas lower values indicate dryness.

SMI = (LSTmax-LST) / (LSTmax-LSTmin)

Soil condition of the basin is categorised as Very Dry (0–0.2), Dry (0.2–0.4), Moderately Dry (0.4–0.6), Moist (0.6–0.8) and Very Moist (0.8–1.0).

Temperature Vegetation Dryness Index (TVDI): The index is derived from the LST–NDVI feature space, in which the lower boundary represents the wet edge and the upper boundary represents the dry edge. For a given NDVI value, the corresponding wet- and dry-edge temperatures were estimated, and TVDI was calculated as:

TVDI= (LST-LSTwet) / (LSTdry-LSTwet)

where LST is the land surface temperature of a pixel, LSTwet is the wet-edge temperature corresponding to the pixel's NDVI, and LSTdry is the dry-edge temperature corresponding to the same NDVI. TVDI values range from 0 to 1, with values approaching 0 indicating relatively wet surface conditions and values approaching 1 indicating increasingly dry conditions. TVDI values are categorised into Normal (0-0.46), Mild drought (0.46-0.57), Moderate drought (0.57-0.76), Severe drought (0.76-0.86) and Extreme drought (0.86-1) (Gu et al., 2026).

Vegetation Health Index (VHI): VHI combines the VCI and TCI to provide an overall drought assessment. It identifies stress levels with values below 40, indicating poor health, and over 60, indicating favourable conditions. Based on Aitekeyeva et al. (2020), VHI values are categorised into Extreme Drought (<10), Severe Drought (10–20), Moderate Drought (20–30), Mild Drought (30–40) and No Drought (≥40).

VHI = α * VCI + (1- α) * TCI

Where: α is a coefficient indicating the proportion of VCI and TCI. Typically, α is set to 0.5, giving equal weight to both parameters.

STUDY AREA

Shiriya River basin covers the area between latitudes 12°31'41.26" N and 12°45'15.98" N and longitudes 74°55'26.73" E and 75°20'55.74" E. Shiriya, the second-longest river in Kasaragod, originates at the foot of the Anne Gundi hills in Dakshina Kannada and discharges into the River Kumbala by joining it. This interstate river is 65 kilometres long; of that, 38 kilometres are situated in the Kasaragod district of Kerala, while the remaining 27 kilometres flow through the Dakshina Kannada district of Karnataka. It is a sixth-order basin; its channel is mostly dendritic, and it is also stretched in shape (Vidya & Manohar, 2022). The present study delineated water boundaries, which show that the Shiriya River basin occupies 579.92 sq.km Basement rocks of this area, the main component of which consists of crystalline charnockites from the Precambrian age, are lateritic soil overlayers (TIES, 2017). The basin is geomorphologically classifiable into hills, midland and lowland. Structural and denudational hills characterise the rugged terrain along the eastern highland segment of the basin. From this region, the midland part gently descends toward the coast and features an undulating topography which consists of a flat lateritic plateau and a valley with a flat bed and a wide mouth, the latter of which also appears.

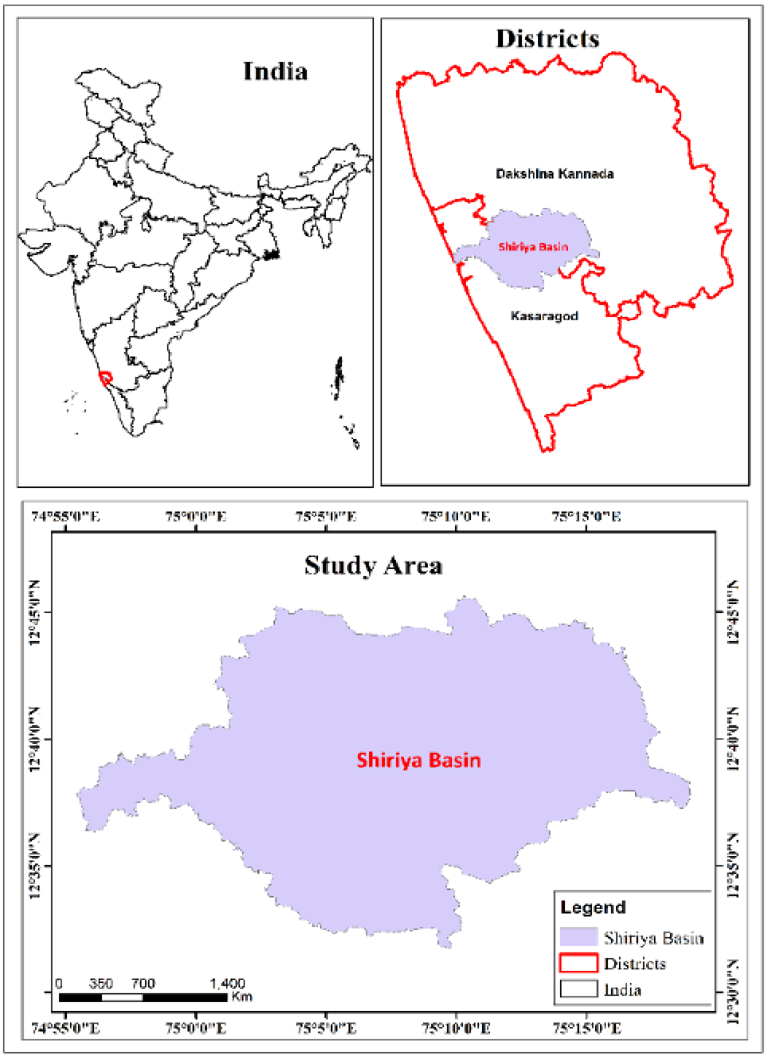

Figure No. 1. Location Map of Study Area

The basin enjoys a warm, humid subtropical climate, and the main monson period, the southwest monsen, brings an annual average rainfall of approximately 3500 mm (Vidya et al., 2024). These characteristics lead to a phenomenon of rapid surface water runoff from the highlands to the lowland seafront within a very short time span (Vidya et al, 2023). The lower parts of the catchment are primarily covered by coconut plantations. In the spots where there is a sufficient supply of water, the cultivation of arecanut and banana, along with coconut, is also prevalent. Paddy farming is not uncommon in these lowland areas. The cashew crop is the most important crop in those pockets where the area is mostly laterite and not enough water has been supplied for the crops.

The hilly terrain areas have extensive rubber plantations. To get water for irrigation in the dry season, temporary bunds are made at the riverbed in December. These bunds are removed shortly before the monsoon season comes so that there is no obstruction to natural river flow, which maintains the moisture regime in the basin (TIES, 2017).

ISSN No. 2454-6186 | DOI: 10.47772/IJRISS | Volume X Issue VII July 2026

RESULT AND DISCUSSION

Pre - monsoon Rainfall Variability and Trend

Pre- monsoon rainfall exhibited pronounced inter-annual variability across the basin during 2002 to 2026 (Fig 4.1). Annual values fluctuated considerably, ranging from relatively low rainfall years to pronounced rainfall peaks. Among the selected assessment years, rainfall was 291.66 mm in 2002, increased to 483.71 mm in 2006, declined to 271.18 mm in 2010 and 287.65 mm in 2014 and subsequently reached 513.21mm in 2018. Rainfall was comparatively lower in 2022 and 2026, accounting for about 338.57 mm and 288.56 mm, respectively. In spite of these fluctuations, Sen's slope showed an overall increasing tendency in pre-monsoon rainfall during the study period. This inter-annual variability is relevant to agricultural drought, as the amount and temporal distribution of pre-monsoon rainfall influence surface and soil moisture availability, vegetation activity and evapotranspiration conditions. Therefore, the positive long-term trend does not necessarily specify the absence of short-term drought stress, particularly during individual years characterised by comparatively low rainfall.

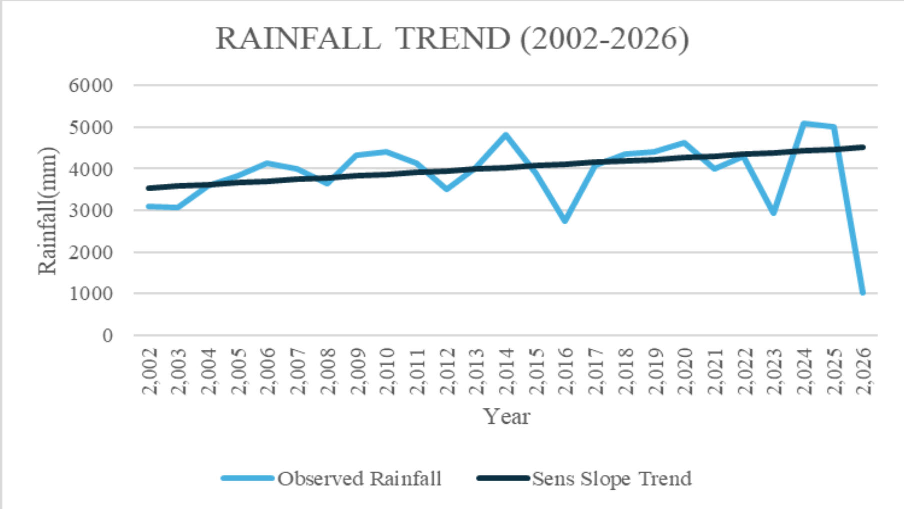

Figure No. 2. Rainfall Variability and Trend

Pre - monsoon Land Surface Temperature trend

Pre-monsoon LST exhibited considerable inter-annual variability during 2002 to 2026, superimposed on a slight declining long-term tendency (Fig 4.2). Among the selected years, mean LST increased from 31.74°C in 2002 to 37.15°C in 2006, representing comparatively strong surface heating. It subsequently declined to 34.45°C in 2010, while values of 35.66°C and 35.17°C were observed in 2014 and 2018, respectively. Lower mean LSTs were recorded during 2022 (34.54°C) and 2016 (34.20°C). Sen's slope indicated an overall declining trend in pre-monsoon LST despite significant year-to-year fluctuations.

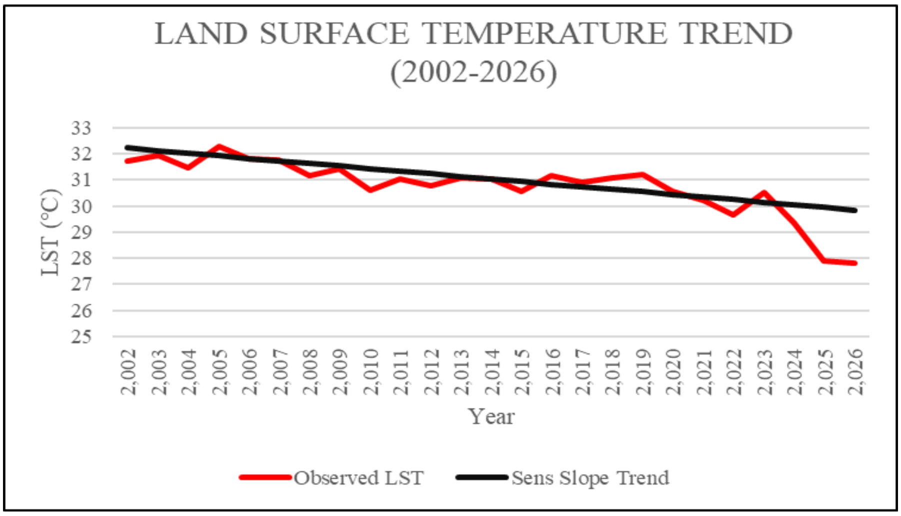

Figure No. 3. Land Surface Temperature trend

ISSN No. 2454-6186 | DOI: 10.47772/IJRISS | Volume X Issue VII July 2026

From an agricultural drought outlook, raised surface temperatures can intensify evaporative demand and accelerate surface moisture depletion, whereas relatively lower LST may indicate reduced thermal stress. Nevertheless, LST is strongly influenced by vegetation cover, surface moisture and LULC, indicating that the observed thermal variability reflects interactions among multiple land surface processes. Therefore, the LST pattern was further interpreted in relation to SMI, VCI, TCI, VHI and TVDI.

NDVI

The NDVI analysis reveals a marked improvement in vegetation condition across the basin from 2002 to 2026. Based on the NDVI classification adopted in this study, the basin was categorised into non-vegetated, sparse vegetation, moderate vegetation, and dense vegetation classes. In 2002, the basin was largely covered by moderate vegetation, but a progressive shift to dense vegetation is evident in subsequent assessment years. Dense vegetation expanded noticeably from 154.74 km2 in 2002 to 356.18 km2 in 2006, and by 2022 it reached its maximum extent of 510.59 km2, accounting for approximately 88% of the basin area. However, a slight reduction was observed in 2026. Correspondingly, moderate vegetation declined considerably from 401.07 km2 in 2002 to 73.32 km2 in 2026, while sparse and non- vegetated surfaces remained comparatively limited. Lower vegetation conditions were more extensive and spatially continuous in 2002, particularly across the western and south-western portions of the basin, while relatively high NDVI conditions were concentrated towards the central and eastern sectors. The 2018 to 2026 maps in particular indicate extensive NDVI surfaces, although localised areas of comparatively low vegetation condition persist, especially towards the western and south-western parts, dotted with rock outcrops. This spatial heterogeneity shows that vegetation response was not uniform throughout the basin.

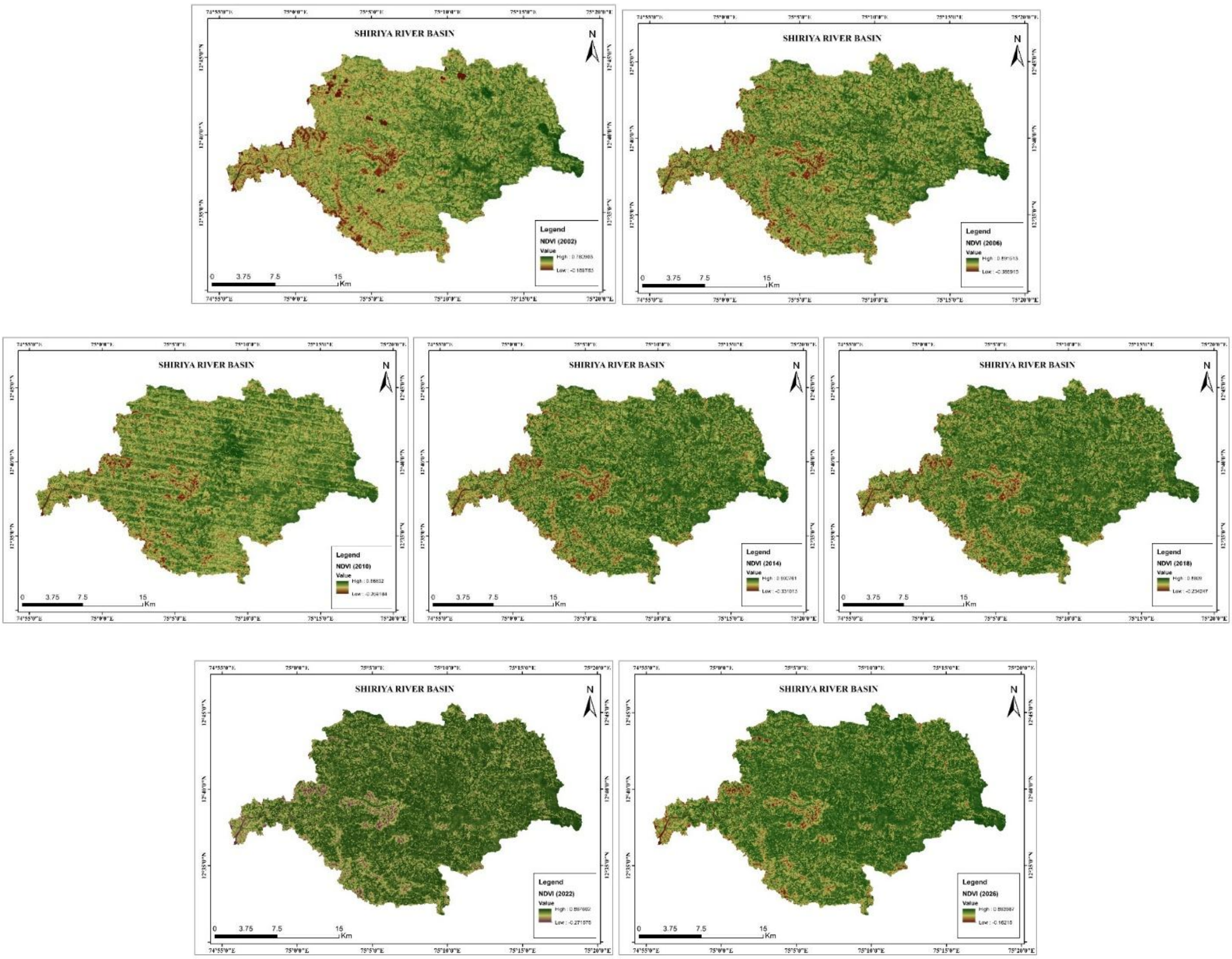

Figure No. 4. Normalised Difference Vegetation Index (2002 to 2026)

ISSN No. 2454-6186 | DOI: 10.47772/IJRISS | Volume X Issue VII July 2026

NDVI Area (km²)	2002	2006	2010	2014	2018	2022	2026
Non-Vegetated	0.19	0.36	0.2	0.34	0.25	0.15	0.17
Sparse Vegetation	23.92	16.77	4.15	5.42	3.16	2.05	2.87
Moderate Vegetation	401.07	206.61	125.17	119.81	104.98	67.13	73.32
Dense Vegetation	154.74	356.18	450.4	454.35	471.53	510.59	503.56
Total	**579.92**	**579.92**	**579.92**	**579.92**	**579.92**	**579.92**	**579.92**

Table No. 2: Normalised Difference Vegetation Index (2002 to 2026)

LST

The land surface temperature pattern of the basin exhibits considerable temporal and spatial variability during 2002 to 2026. The maps indicate a general transition from relatively heterogeneous thermal conditions in the earlier years towards the increasing dominance of moderate surface temperature in the later period. Warmer surfaces are not uniformly distributed across the basin; instead, distinct high-temperature pockets occur particularly in the rock outcrops and adjacent areas in the western and south-western portions and along some central zones, while comparatively lower temperatures are more prominent towards the eastern and north-eastern parts.

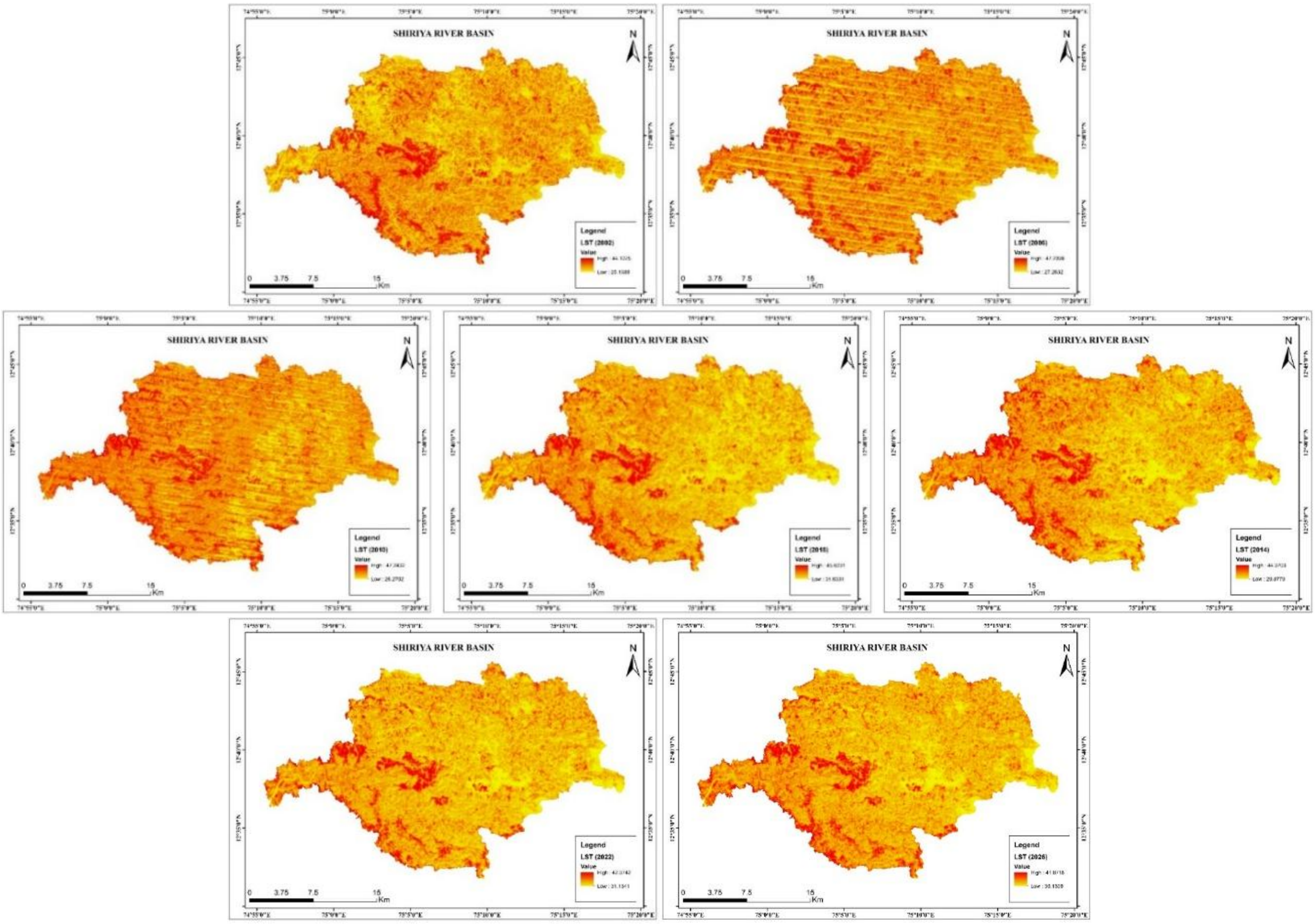

Figure No. 5. Land Surface Temperature (2002 to 2026)

ISSN No. 2454-6186 | DOI: 10.47772/IJRISS | Volume X Issue VII July 2026

LST Area (km²)	2002	2006	2010	2014	2018	2022	2026
Very Low	83.62	4.71	10.52	0	0	0	0
Low	266.78	105.15	100.25	97.61	10.02	29.46	92.71
Moderate	155.84	262.18	281.13	345.45	337.37	461.46	413.73
High	49.56	142.59	133	101.61	182.25	72.34	60.2
Very High	24.12	65.29	55.02	35.25	50.28	16.66	13.28
Total	**579.92**	**579.92**	**579.92**	**579.92**	**579.92**	**579.92**	**579.92**

Table No. 3: Land Surface Temperature (2002 to 2026)

The temporal pattern is characterised by fluctuations rather than a continuous warming trend. Comparatively high thermal stress is evident during 2006 and 2018, when high and very high LST conditions become more extensive. In contrast, 2022 and 2026 show a pronounced dominance of moderate temperature conditions accompanied by a contraction of the highest temperature surfaces. Another notable feature is the disappearance of the very low temperature category after the earlier observation years. Overall, the LST values reveal a dynamic thermal regime rather than a unidirectional temperature trend, with alternating periods of enhanced and reduced surface heating. The thermal variations complement the vegetation dynamics identified through NDVI.

VCI

Vegetation Condition Index indicates a pronounced improvement in vegetation condition across the basin between 2002 and 2026. VCI range classification. The year 2002 represents the most severe vegetation stress condition among the selected years, with extreme drought occupying approximately 92.3 % of the basin. By 2006, extreme drought had reduced considerably, although extreme, severe and moderate drought conditions still occupied a substantial part of the basin. An additional reduction in vegetation stress occurred during 2010 and 2014, accompanied by an expansion of the light-drought and no-drought classes.

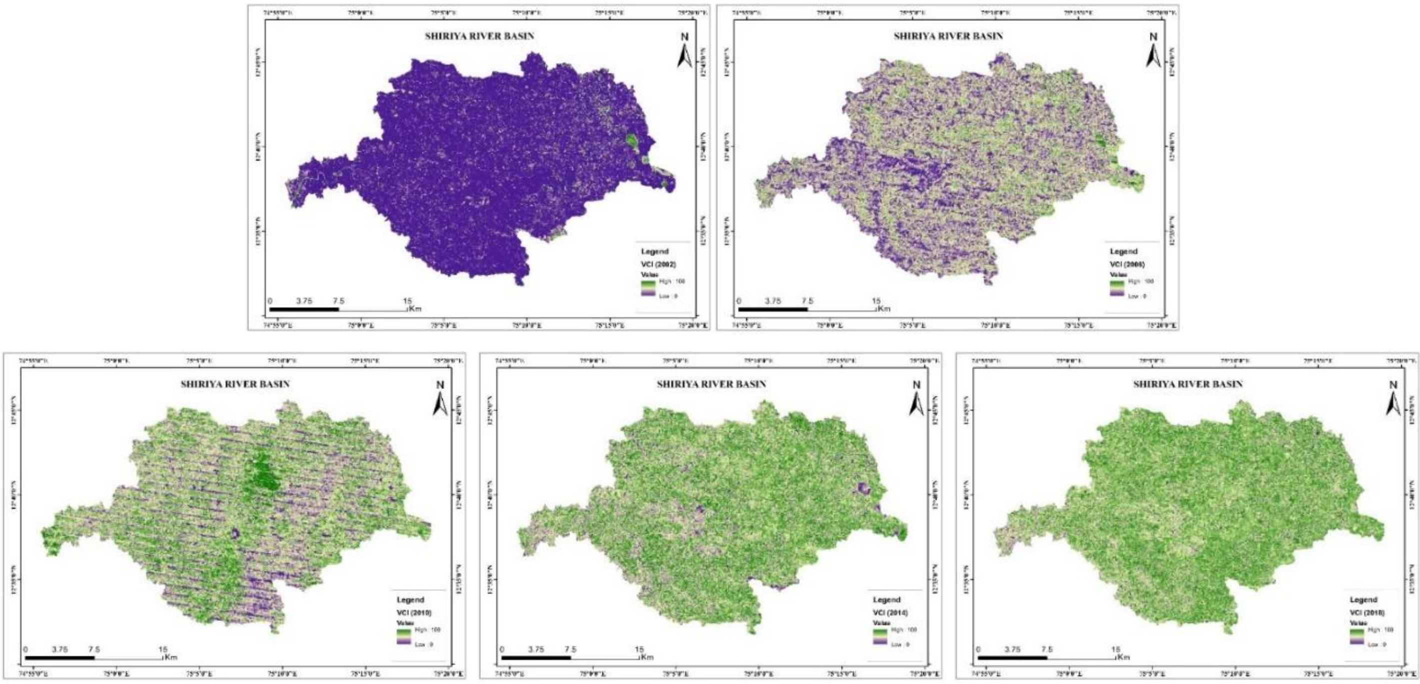

INTERNATIONAL JOURNAL OF RESEARCH AND INNOVATION IN SOCIAL SCIENCE (IJRISS)
ISSN No. 2454-6186 | DOI: 10.47772/IJRISS | Volume X Issue VII July 2026

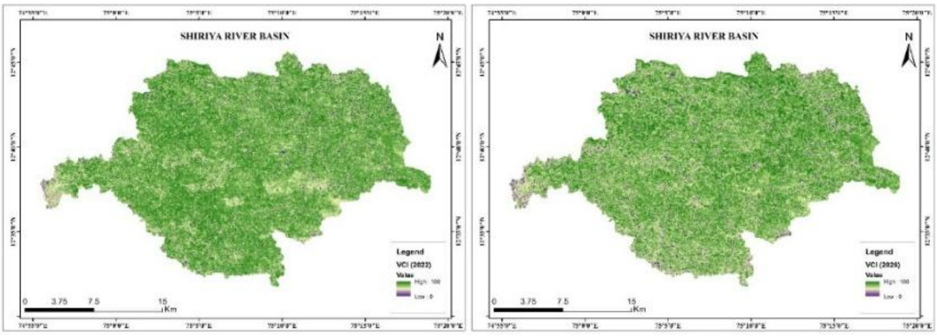

Figure No. 6. Vegetation Condition Index (2002 to 2026)

VCI Area (km²)	2002	2006	2010	2014	2018	2022	2026
Extreme Drought	535.05	163.99	55.87	24.11	8.92	5.82	10.54
Severe Drought	29.77	192.46	109.87	58.23	25.97	13.87	23.78
Moderate Drought	11.3	167.67	160.69	125.06	99.66	45.2	67.26
Light Drought	3.6	48.59	167.35	224.6	310.14	243.53	256.54
No Drought	0.2	7.21	86.14	147.92	135.23	271.5	221.8
Total	**579.92**	**579.92**	**579.92**	**579.92**	**579.92**	**579.92**	**579.92**

Table No. 4: Vegetation Condition Index (2002 to 2026)

The improvement is evident after 2014. The most favourable vegetation condition was observed in 2022 when the no-drought category expanded to 271.50 km2 (approximately 46.8%), while extreme and severe drought together accounted for only about 3.4 % of the basin. The spatial maps similarly show a progressive transition from predominantly low VCI conditions in 2002 towards widespread high VCI conditions in 2018 and 2022. In 2026, however, no-drought classes decreased slightly compared with 2022, while moderate, severe and extreme drought classes increased slightly, indicating a modest deterioration in vegetation condition rather than a return to the severe conditions observed during the earlier years. This temporal behaviour is broadly consistent with the NDVI results.

TCI

The temperature condition index shows that thermal stress did not remain constant throughout the study period. The basin shifted between relatively favourable conditions in 2002 and episodes of widespread thermal stress later in the year. The most prominent deterioration occurred during 2006 and 2010, when severe and very severe drought conditions expanded substantially across the basin. Thermal conditions improved markedly by 2014, with moderate drought becoming dominant and very severe drought declining considerably. However, another distinct period of thermal stress emerged in 2018, characterised by a strong expansion of the severe drought category. This corresponds with the relatively elevated LST conditions observed for the same year, indicating that increased surface temperature translated into greater thermal stress. A substantial improvement is evident in 2022 and 2026. Very severe drought became almost negligible, while the basin was predominantly characterised by moderate drought conditions mainly in eastern parts. By 2026, the expansion of the very low drought category further indicates an improvement in thermal conditions in several parts of the basin. Nevertheless, the persistence of moderate drought over a large area shows that thermal stress has not disappeared completely, but it moves between western and eastern parts of the basin.

ISSN No. 2454-6186 | DOI: 10.47772/IJRISS | Volume X Issue VII July 2026

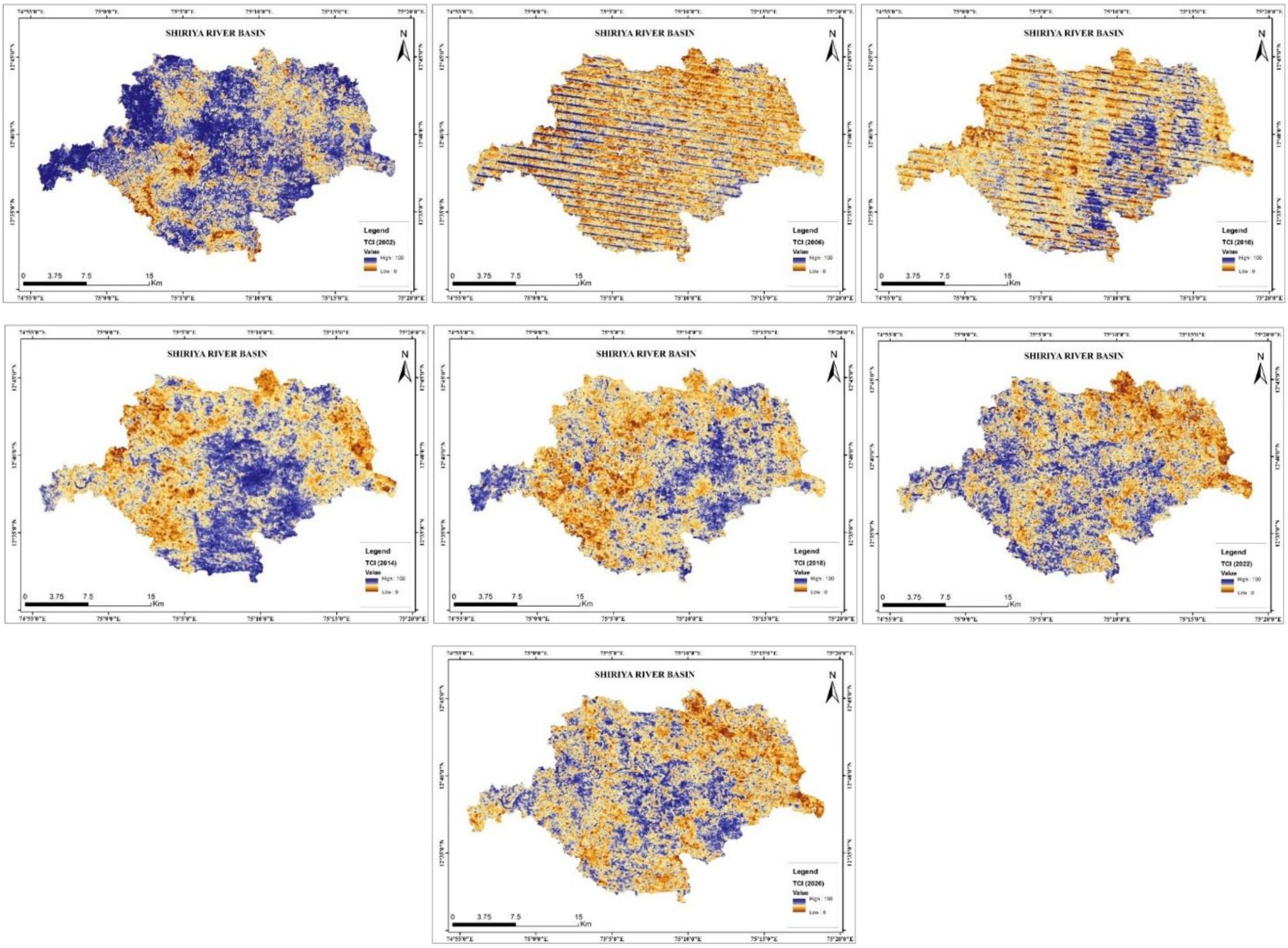

Figure No. 7. Temperature Condition Index (2002 to 2026)

TCI Area (km²)	2002	2006	2010	2014	2018	2022	2026
Very Severe Drought	3.7	50.19	45.33	5.31	12.05	0.33	0.26
Severe Drought	30	199.59	162.11	135.2	329.44	73.99	30.02
Moderate Drought	140.81	227.78	262.21	344.75	233.18	447.11	408.31
Very Low Drought	240.07	73.2	81.44	93.52	5.25	58.45	140.84
No Drought	165.34	29.16	28.83	1.14	0	0.04	0.49
Total	**579.92**	**579.92**	**579.92**	**579.92**	**579.92**	**579.92**	**579.92**

Table No. 5: Temperature Condition Index (2002 to 2026)

SMI

The soil moisture index indicates a general improvement in moisture conditions in the Shiriya River Basin over the study period, although substantial inter-annual variability is evident. The earlier years, particularly 2006 and 2010, show comparatively greater moisture stress, with dry and moderately dry conditions occupying a larger proportion of the basin. The situation changes markedly from 2014 onward, when moist and very moist conditions become increasingly dominant. This improvement is particularly evident in 2018 and 2022, with 2022 representing the most favourable overall moisture condition among the analysed years. In 2026, the moist category expands further, although the very moist area declines compared with 2022, indicating a redistribution

ISSN No. 2454-6186 | DOI: 10.47772/IJRISS | Volume X Issue VII July 2026

from very high moisture conditions towards moderately favourable moisture availability rather than a major drying of the basin. Lower SMI values are repeatedly concentrated in the western to southwestern portions, whereas comparatively higher soil moisture conditions dominate much of the central and eastern sectors.

SMI Area (km²)	**2002**	**2006**	**2010**	**2014**	**2018**	**2022**	**2026**
Very Dry	21.67	23.91	21.2	20.88	19.69	15.63	17.38
Dry	42.18	57.72	55.83	34.83	30.16	25.26	28.99
Moderate Dry	124.13	170.09	201.57	99.22	87.44	66.24	77.38
Moist	253	255.31	252.59	254.23	262.13	271.48	293.93
Very Moist	138.94	72.89	48.73	170.76	180.5	201.31	162.24
Total	**579.92**	**579.92**	**579.92**	**579.92**	**579.92**	**579.92**	**579.92**

Table No. 6: Soil Moisture Index (2002 to 2026)

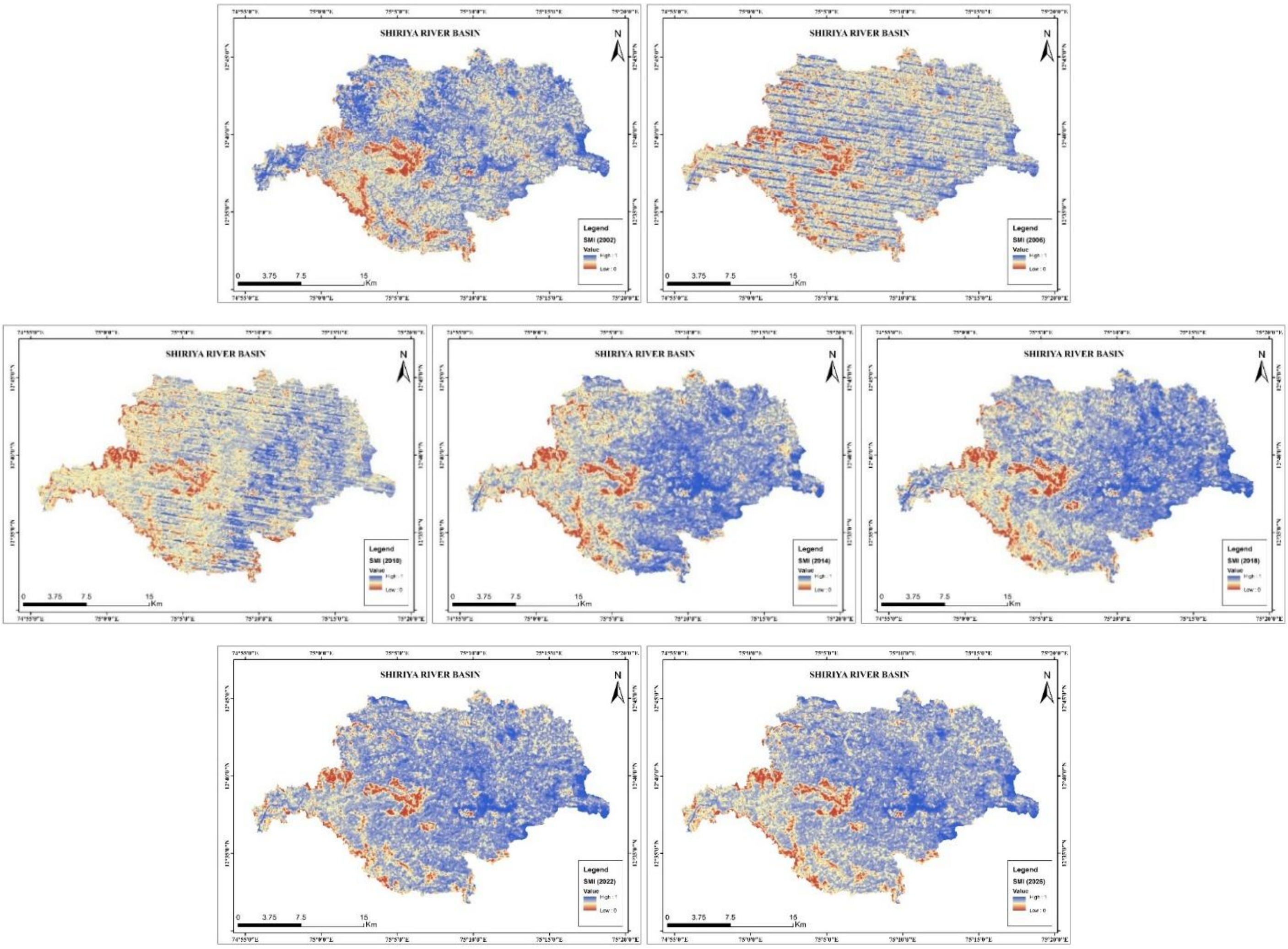

Figure No. 8. Soil Moisture Index (2002 to 2026)

VHI

The VHI analysis reveals a pronounced improvement in vegetation health across the basin during the study years. In 2002, drought conditions ranging from mild to extreme affected approximately 371.94 km² of the basin, declining to only 15.95 km2 in 2022. Consequently, the non-drought category expanded from 207.98 km2 in 2002 to 563.97 km2 in 2022. A slight increase in drought-affected area was observed in 2026 (21.97 km2); however, the basin remained predominantly under non-drought conditions, covering 557.95 km2. Overall, the

ISSN No. 2454-6186 | DOI: 10.47772/IJRISS | Volume X Issue VII July 2026

VHI results indicate a substantial long-term reduction in vegetation stress, with 2022exhibiting the most favourable vegetation health condition among the selected years.

VHI Area (km²)	2002	2006	2010	2014	2018	2022	2026
Extreme Drought	3.03	21.38	7.36	0.82	0.69	0.09	0.09
Severe Drought	26.1	63.55	17.91	6.32	3.47	1.14	1.41
Moderate Drought	122.15	94.57	39.82	19.46	10.6	3.81	5.88
Mild Drought	220.66	119.73	78.07	45.31	36.96	9.97	14.59
No Drought	207.98	280.69	436.76	508.01	528.2	564.91	557.95
Total	**579.92**	**579.92**	**579.92**	**579.92**	**579.92**	**579.92**	**579.92**

Table No. 7: Vegetation Health Index (2002 to 2026)

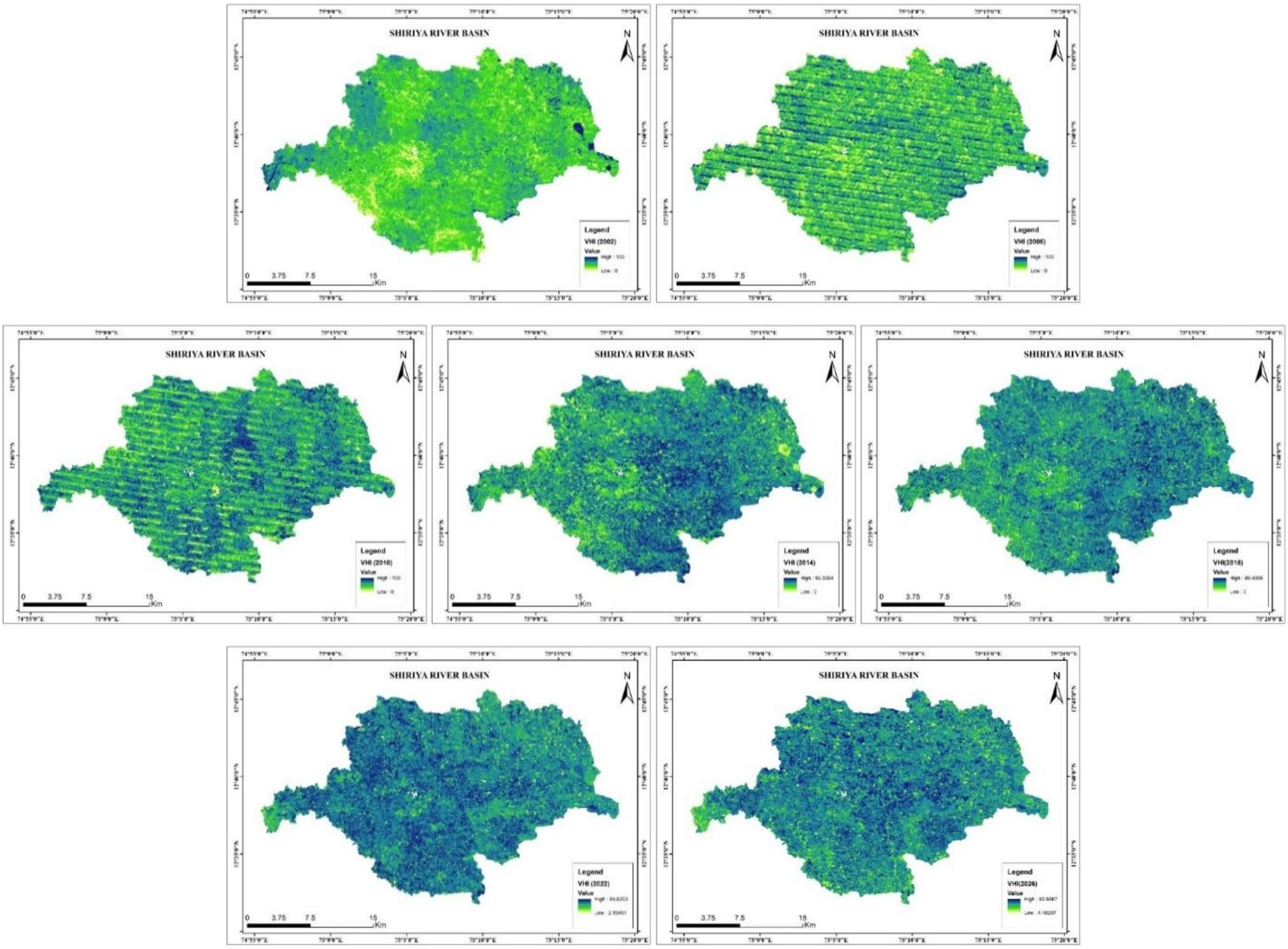

Figure No. 9. Vegetation Health Index (2002 to 2026)

TVDI

The TVDI analysis reveals a clear long-term reduction in drought stress across the basin. In the early years, particularly 2002 and 2006, drought conditions were relatively widespread, but from 2010 onwards, a progressive improvement is evident. This improvement continued through 2014 and 2018 and became most pronounced in 2022, when normal conditions occupied the largest extent of the basin. The spatial maps similarly indicate a gradual shift towards lower TVDI conditions over time, although pockets of higher dryness persisted in some parts of the basin. In 2026, a slight reversal is observed compared with 2022, with a modest increase in the different drought categories and a corresponding decline in the normal category. In short, the TVDI results indicate a long-term decline in surface moisture and thermal drought stress, interrupted by a minor deterioration in 2026.

ISSN No. 2454-6186 | DOI: 10.47772/IJRISS | Volume X Issue VII July 2026

TVDI Area (km²)	2002	2006	2010	2014	2018	2022	2026
Normal	264.32	254.93	335.77	389.59	424.5	462.64	449.21
Mild Drought	84.61	98.64	69.94	60.14	49.99	36.42	40.88
Moderate Drought	121.03	135.08	90.35	62.22	44.77	35.84	39.78
Severe Drought	41.52	41.58	31.03	20.18	14.9	11.66	13.8
Extreme Drought	68.44	49.69	52.83	47.79	45.76	33.36	36.25
Total	**579.92**	**579.92**	**579.92**	**579.92**	**579.92**	**579.92**	**579.92**

Table No. 8: Temperature Vegetation Dryness Index (2002 to 2026)

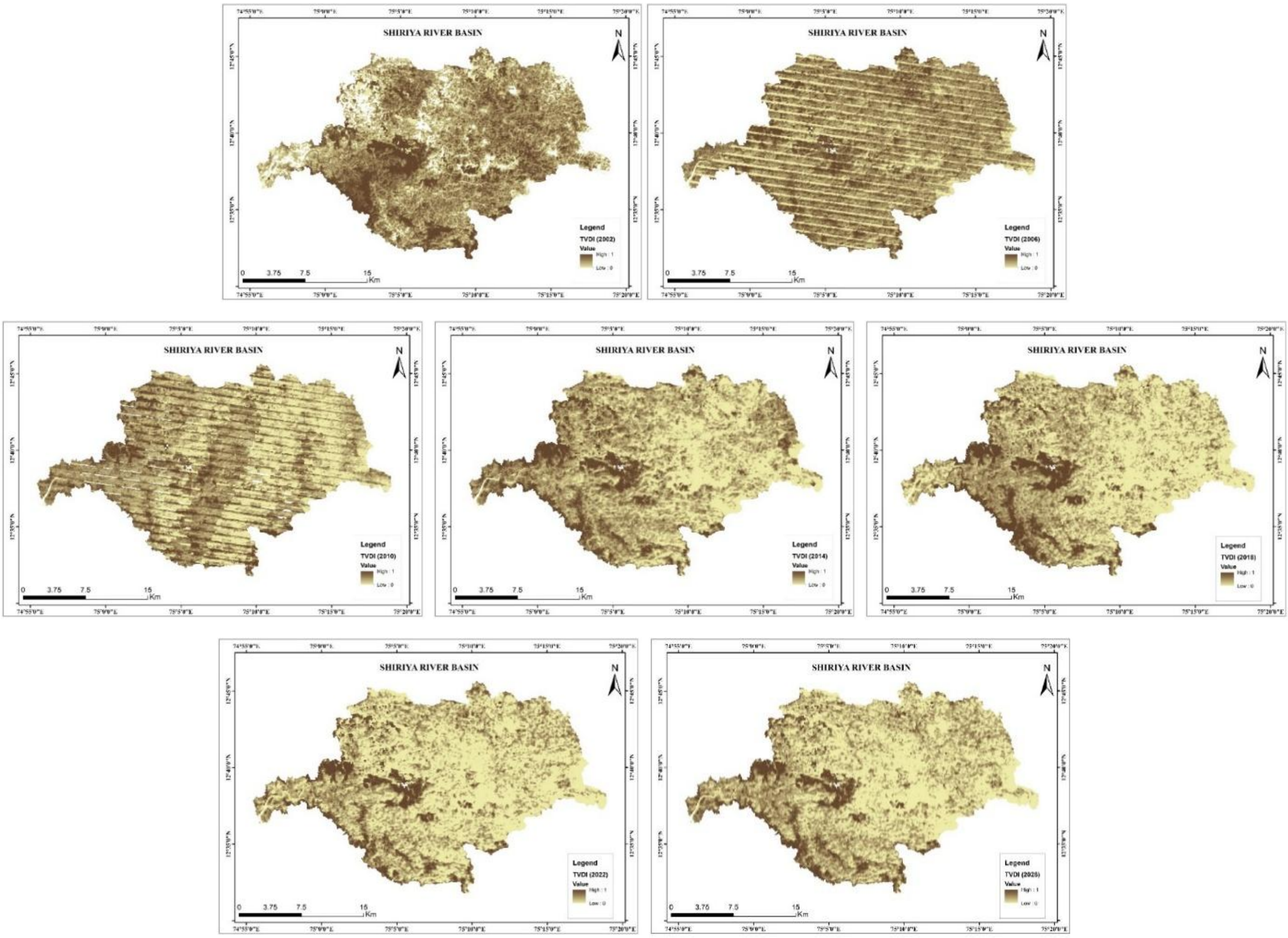

Figure No. 10. Temperature Vegetation Dryness Index (2002 to 2026)

LULC CHANGE

2002: Overall, the basin is dominated by dark green forest with patches of pale yellow agriculture in moderately sized clusters throughout the northern, central and south-western parts of the basin, while the red built-up and black barren areas are confined to the western river outlet and thinner streaks scattered inside the basin, with one large barren spot in the west-central hills.

2006: Similar to the 2002 map, but with a more consolidated patch of barren land in the central western part along the river and the same smaller cluster of built-up areas in the western basin outskirts, while the agricultural areas are fragmented all along the northern and southern boundaries.

2010: Overall, this map is almost identical to the previous one, with the same pattern of forest, agriculture, barren and built-up land, save for the possibly more defined rectangular shapes of various land covers, suggesting that the same classification might have been used.

2014: Forest appears to become more consolidated and occupy larger areas, while the agriculture patches become more isolated and linear along the roadways, with barren land areas also apparent in the same western centre hills, and the built-up areas also take the form of thin lines along the roads between forested areas.

2018: Agriculture appears to be more prominent, taking the form of large patches of yellow along the northern and eastern basin boundaries and near the western river outlet, while barren and built-up areas are still localised around the western centre hills, with forest dominating the areas in between.

2022: Similar to the 2018 map, but with slightly smaller agricultural areas and more pronounced red line streaks of built-up areas cutting through the forest, while the same general pattern of land cover is observed with minor changes to the sizes and shapes of individual patches.

2026: The latest map appears to depict an overall increase in barren land in contrast to previous years, as it is now distributed as more widely dispersed stippling across the basin, as opposed to the localized cluster in the centre western hills in 2018, with the built-up areas increasing overall in number and connected by roadways, while the agriculture areas are also smaller and more fragmented than in 2018. Forest, while still the dominant land cover type, also decreases in prominence compared to 2018 and appears less consolidated.

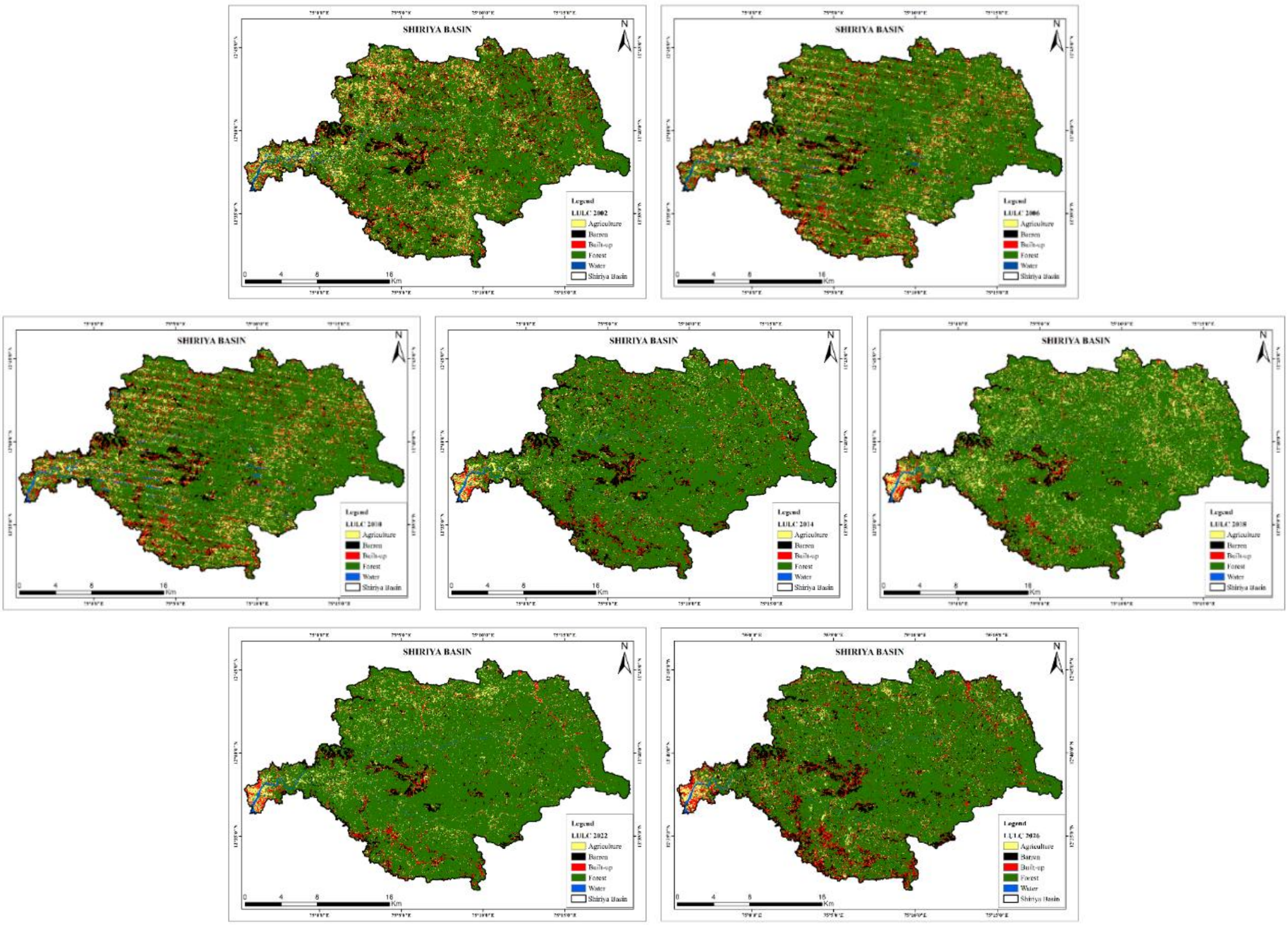

Figure No. 11. Land Use and Land Cover (LULC) (2002 to 2026)

Sl. No.	Class	2002	2006	2010	2014	2018	2022	2026
1	Agriculture	74.2	67.71	62.71	37.47	77.65	41.73	35.81
2	Barren	66.29	53.44	47.44	30.61	41.44	36.63	63.62
3	Built-up	59.23	58.04	63.04	63.69	23.5	25.65	47.83
4	Forest	376.17	394.97	401.97	445.09	434.75	473.03	429.69
5	Water	4.03	5.76	4.76	3.06	2.59	2.88	2.97
Total		**579.92**	**579.92**	**579.92**	**579.92**	**579.92**	**579.92**	**579.92**

Table No. 9: Land Use and Land Cover Change (2002 to 2026)

The figures confirm some of the observations made from the maps, namely that the distribution of the different land covers follows a pattern of change rather than consistent increases or decreases. For instance, agriculture reaches its peak in 2018 at 77.65 sq. km but decreases drastically to 35.81 sq. km by 2026. Barren land peaks at 66.29 sq. km in 2002 but drops to 41.44 sq. km in 2018 before climbing steeply to 63.62 sq. km in 2026. As for the built-up areas, they decrease gradually from 59.23 sq. km in 2002 to a low of 23.50 sq. km in 2018 before spiking to 47.83 sq. km in 2026. The area covered in forests peaks in 2022 at 473.03 sq. km but drops slightly to 429.69 sq. km in 2026. Finally, the area covered by water decreases overall from 4.03 sq. km in 2002 to below 3 sq. km in 2014 and remains roughly stable for the following years.

CONCLUSION

The composite analysis of rainfall, land surface temperature (LST), vegetation, and drought indices from 2002 to 2026 revealed significant changes in the hydrological and ecological characteristics of the Shiriya River Basin. While rainfall varied significantly between years, it appeared to demonstrate an overall increasing trend throughout the study period. But, LST trends showed a gradual decrease, although LST showed pronounced highs in 2006 and 2018. In turn, the majority of vegetation- and moisture-related indices (NDVI, VCI, VHI, TCI, SMI, and TVDI) demonstrated an improvement in vegetation conditions and moisture regime. Thus, the Shiriya River Basin was covered predominantly by densely vegetated land classes during 2010 – 2022, with some signs of vegetation drought. Moreover, compared to the other years under study, 2022 can be considered the best year for the region as it was characterised by the lowest levels of thermal and moisture stress.

Contrarily, the year 2026 can be preliminarily identified as a year of deterioration, as a majority of the considered indices showed a slight decrease in vegetation and moisture conditions, and the first signs of local thermal and vegetation droughts were detected, suggesting the need for continued monitoring. Additionally, the analysis of land use/land cover changes revealed that the transformation of barren lands and built-up areas increased considerably. Specifically, barren lands increased by 12%, accounting for 63.62 km 2, while built-up areas nearly doubled, reaching 47.83 km 2 in 2026. In contrast, the area of agricultural land was reduced to 35.81 km 2 in 2026. Though forests remained the predominant land cover type, their areal extent also decreased, and their distribution became fragmented.

In general, the current ecological trends in the Shiriya River Basin can be considered positive, as they are primarily governed by increased rainfall, which improved the majority of vegetation- and moisture-related indices. However, the changes detected in 2026 suggest the initiation of large-scale environmental deterioration processes associated with the transformation of the regional land cover system. The continuous monitoring of the study area using high-resolution satellite sensors will allow for elucidating the short-term trends and detecting long-term environmental changes that may affect the sustainability of the Shiriya River Basin.

REFERENCES

1. Aitekeyeva, N., Li, X., Guo, H., Wu, W., Shirazi, Z., Ilyas, S., Yegizbayeva, A., & Hategekimana, Y. (2020). Drought risk assessment in cultivated areas of Central Asia using MODIS time-series data. *Water (Switzerland), 12*(6). https://doi.org/10.3390/W12061738
2. Almeida-Ñauñay, S., et al. (2022). Vegetation monitoring using NDVI derived from remote sensing data: Applications and challenges. Remote Sensing Applications: Society and Environment, 25, 100687. https://doi.org/10.1016/j.rsase.2021.100687
3. American Meteorological Society. (1997). Meteorological drought—Policy statement. American Meteorological Society. https://www.ametsoc.org
4. Bento, V. A., Gouveia, C. M., da Câmara, C. C., & Trigo, I. F. (2018). A climatological assessment of drought impact on vegetation health index. Agricultural and Forest Meteorology, 259, 286–295. https://doi.org/10.1016/j.agrformet.2018.05.014
5. Bento, V. A., Gouveia, C. M., DaCamara, C. C., Libonati, R., & Trigo, I. F. (2020). The roles of NDVI and Land Surface Temperature when using the Vegetation Health Index over dry regions. *Global and Planetary Change*, *190*, 103198. https://doi.org/10.1016/J.GLOPLACHA.2020.103198
6. Canedo-Rosso, C., Hochrainer-Stigler, S., Pflug, G., Condori, B., & Berndtsson, R. (2021). Drought impact in the Bolivian Altiplano agriculture associated with the El Niño-Southern Oscillation using

satellite imagery data. *Natural Hazards and Earth System Sciences*, *21*(3), 995–1010. https://doi.org/10.5194/nhess-21-995-2021

7. Chakraborty, A., & Sehgal, V. K. (2010). *Assessment of Agricultural Drought Using MODIS Derived Normalized Difference Water Index*. Retrieved www.cr.usgs.gov./pub/imswelcome/
8. Chere, Z., Abegaz, A., Tamene, L., & Abera, W. (2022). Modeling and mapping the spatiotemporal variation in agricultural drought based on a satellite-derived vegetation health index across the highlands of Ethiopia. *Modeling Earth Systems and Environment*, *8*(4), 4539–4552. https://doi.org/10.1007/s40808-022-01439-x
9. Dai, A. (2013). Increasing drought under global warming in observations and models. Nature Climate Change, 3(1), 52–58. https://doi.org/10.1038/nclimate1633
10. Das, S., Choudhury, R., & Nanda, S. (2013). GEOSPATIAL ASSESSMENT OF AGRICULTURAL DROUGHT (A CASE STUDY OF BANKURA DISTRICT, WEST BENGAL). In *International Journal of Agricultural Science and Research* (Vol. 3).
11. Dudumashe, N., & Thomas, A. (2020, December 2). *ASSESSMENT OF LAND SURFACE TEMPERATURE AND DROUGHT INDICES FOR THE KLERKSDORP-ORKNEY-STILFONTEIN-HARTEBEESFONTEIN (KOSH) REGION*. https://doi.org/10.25686/7230.2020.6.58828
12. Boudjemline, F., & Benlabiod, D. (2022). *The use of Standardized Precipitation Index values (SPI) and MODIS vegetation indices to assess drought in steppe regions, Algeria*.
13. Gu, Z., Xu, G., Feng, L., Li, Y., Ji, K., & Reheman, M. (2026). Spatiotemporal dynamics and driving factors of drought in the Yellow River Basin (Henan section): insights from TVDI analysis. *Frontiers in Ecology and Evolution*, *14*.
14. Hang, Q., Guo, H., Meng, X., Wang, W., Cao, Y., Liu, R., De Maeyer, P., & Wang, Y. (2024). Optimising the Vegetation Health Index for Agricultural Drought Monitoring: Evaluation and Application in the Yellow River Basin. *Remote Sensing*, *16*(23), 4507. https://doi.org/10.3390/rs16234507
15. Huang, D., Ma, T., Liu, J., & Zhang, J. (2025). Agricultural drought monitoring using modified TVDI and dynamic drought thresholds in the upper and middle Huai River Basin, China. Journal of Hydrology: Regional Studies, 57, 102069. https://doi.org/10.1016/J.EJRH.2024.102069
16. Kao, S. C., & Govindaraju, R. S. (2010). A copula-based joint deficit index for droughts. Journal of Hydrology, 380(1–2), 121–134. https://doi.org/10.1016/j.jhydrol.2009.10.029
17. Kogan, F. N. (1995a). Application of vegetation index and brightness temperature for drought detection. Advances in Space Research, 15(11), 91–100. https://doi.org/10.1016/0273-1177(95)00079-T
18. Kogan, F. N. (1995b). Droughts of the late 1980s in the United States as derived from NOAA polar-orbiting satellite data. Bulletin of the American Meteorological Society, 76(5), 655–668. https://doi.org/10.1175/1520-0477(1995)076<0655: DOTLIT>2.0.CO;2
19. Kourouma, K., et al. (2021). Monitoring vegetation dynamics using NDVI from satellite imagery. Remote Sensing Applications: Society and Environment, 23, 100567. https://doi.org/10.1016/j.rsase.2021.100567
20. Laksono, A., Saputri, A. A., Pratiwi, C. I. B., Arkan, M. Z., & Putri, R. F. (2020). Vegetation covers change and its impact on Barchan Dune morphology in Parangtritis Coast, Indonesia. *E3S Web of Conferences*, *200*. https://doi.org/10.1051/e3sconf/202020002026
21. Li, Z. L., Wu, H., Duan, S. B., Zhao, W., Ren, H., Liu, X., Leng, P., Tang, R., Ye, X., Zhu, J., Sun, Y., Si, M., Liu, M., Li, J., Zhang, X., Shang, G., Tang, B. H., Yan, G., & Zhou, C. (2023). Satellite Remote Sensing of Global Land Surface Temperature: Definition, Methods, Products, and Applications. In *Reviews of Geophysics* (Vol. 61, Number 1). John Wiley and Sons Inc. https://doi.org/10.1029/2022RG000777
22. Liu, Y., & Yue, H. (2018). The Temperature Vegetation Dryness Index (TVDI) Based on Bi-Parabolic NDVI-Ts Space and Gradient-Based Structural Similarity (GSSIM) for Long-Term Drought Assessment Across Shaanxi Province, China (2000–2016). *Remote Sensing*, *10*(6), 959. https://doi.org/10.3390/rs10060959
23. Liu, Y., Wu, L., & Yue, H. (2015). Biparabolic NDVI-T_s Space and Soil Moisture Remote Sensing in an Arid and Semi-arid Area. *Canadian Journal of Remote Sensing*, *41*(3), 159–169. https://doi.org/10.1080/07038992.2015.1065705

24. Mayouf, R., & Hanafi, M. T. (2024). Integrating remote sensing modeling for drought assessment and vegetation monitoring in El Tarf, Algeria: a 40-year analysis. *STUDIES IN ENGINEERING AND EXACT SCIENCES*, *5*(2), e9690. https://doi.org/10.54021/seesv5n2-390sh
25. McKee, T. B., Doesken, N. J., & Kleist, J. (1993). The relationship of drought frequency and duration to time scales. Proceedings of the 8th Conference on Applied Climatology, 179–184.
26. Meneses-Tovar, C. L. (2011). NDVI as an indicator of degradation and desertification. Unasylva, 62(238), 39–46.
27. Mistry, P. B., & Suryanarayana, T. M. V. (2023). Assessment & monitoring of agricultural drought indices using remote sensing techniques and their inter-comparison. Ecological Perspective, 3(1), 1–8. https://doi.org/10.53463/ecopers.20230171
28. Palagiri, H., & Pal, M. (2023). Agricultural Drought Monitoring using Satellite-based Surface Soil Moisture Data. In EGU General Assembly Conference Abstracts (pp. EGU-621).
29. Rahman, G., Khalid, S., Arshad, S., Moazzam, M. F. U., & Kwon, H. H. (2025). Remote sensing-based spatiotemporal assessment of agricultural drought and its impact on crop yields in Punjab, Pakistan. *Scientific Reports*, *15*(1). https://doi.org/10.1038/s41598-025-06095-6
30. Saha, A., Patil, M., Goyal, V. C., & Rathore, D. S. (2019). Assessment and Impact of Soil Moisture Index in Agricultural Drought Estimation Using Remote Sensing and GIS Techniques. *Proceedings*, *7*(1), 2. https://doi.org/10.3390/ECWS-3-05802
31. Serban, C., & Maftei, C. (2025). Remote Sensing Evaluation of Drought Effects on Crop Yields Across Dobrogea, Romania, Using Vegetation Health Index (VHI). *Agriculture (Switzerland)*, *15*(7). https://doi.org/10.3390/agriculture15070668
32. Shahzaman, M., Zhu, W., Bilal, M., Habtemicheal, B. A., Mustafa, F., Arshad, M., Ullah, I., Ishfaq, S., & Iqbal, R. (2021). Remote sensing indices for spatial monitoring of agricultural drought in south asian countries. *Remote Sensing*, *13*(11). https://doi.org/10.3390/rs13112059
33. Shastri, J. N., & Mujumdar, S. S. (2025). Use of Satellite-Based Remote Sensing Indices for Agricultural Drought Monitoring in Saurashtra, Gujarat. *Meteorological Applications*, *32*(6). https://doi.org/10.1002/met.70132
34. Shoumik, B. A. Al, Khan, M. Z., & Islam, M. S. (2023). Spatio-temporal characteristics of meteorological and agricultural drought indices and their dynamic relationships during the pre-monsoon season in drought-prone region of Bangladesh. *Environmental Challenges*, *11*. https://doi.org/10.1016/j.envc.2023.100695
35. Šorman, A. Ü., Mehr, A. D., & Hadi, S. J. (2018). Study on spatial-temporal variations of meteorological-agricultural droughts in Turkey. *International Archives of the Photogrammetry, Remote Sensing and Spatial Information Sciences - ISPRS Archives*, *42*(3W4), 483–490. https://doi.org/10.5194/isprs-archives-XLII-3-W4-483-2018
36. Sreekesh, S., Kaur, N., and Sreerama Naik, S. R. (2019). Agricultural Drought and Soil Moisture Analysis Using Satellite Image-Based Indices, Int. Arch. Photogramm. Remote Sens. Spatial Inf. Sci., XLII-3/W6, 507–514, https://doi.org/10.5194/isprs-archives-XLII-3-W6-507-2019.
37. Sun, D., Li, Y., Zhan, X., Yang, C., & Yang, R. (2021). Integrating optical and microwave satellite observations for high resolution soil moisture estimate and applications in CONUS drought analyses. *Journal of Geography and Cartography*, *4*(1), 93. https://doi.org/10.24294/jgc.v4i1.1313
38. Tropical Institute of Ecological Sciences (TIES). (2017). *Reconnaissance Survey Report: Shiriya River and Yelkanna River, Kasaragod District.* Tropical Institute of Ecological Sciences (TIES), Kottayam, Kerala.
39. Vallejo-Villalta, I., Rodríguez-Navas, E., & Márquez-Pérez, J. (2019). Mapping forest fire risk at a local scale—A case study in Andalusia (Spain). *Environments - MDPI*, *6*(3). https://doi.org/10.3390/environments6030030
40. Vidya KM, Manoharan AN. (2022) Morphometric Analysis for Sustainable Development of Watersheds Using Multisensor Satellite Data: A Case Study from Shiriya River Basin. *Indian Journal of Science and Technology*. 15(35): 1691-1702. https://doi.org/10.17485/IJST/v15i35.994
41. Vidya, K. M., Manoharan, A. N., & Deepchand, V. (2023). Investigating the Tectonic and Structural Controls on the Geomorphic Evolution of Shiriya River Basin, Southern India. *Journal of the Geological Society of India*, *99*, 1292–1304. doi:https://doi.org/10.1007/s12594-023-2463-1

42. Vidya, K. M., Manoharan, A. N., Suchitra, B., & Shyni, M. (2024). Combination of remote sensing, GIS, AHP techniques and geophysical data to delineate groundwater potential zones in the Shiriya River Basin, South India. Geosystems and Geoenvironment, 3(4), 100294. https://doi.org/10.1016/j.geogeo.2024.100294
43. Wang, Z., Guo, P., Wan, H., Tian, F., & Wang, L. (2020). Integration of microwave and optical/infrared derived datasets from multi-satellite products for drought monitoring. *Water (Switzerland)*, *12*(5). https://doi.org/10.3390/w12051504
44. Yu, X., & Guo, X. (2023). Inter-annual drought monitoring in northern mixed grasslands by a revised vegetation health index from historical Landsat imagery. *Journal of Arid Environments*, *213*, 104964. https://doi.org/10.1016/J.JARIDENV.2023.104964
45. Zeng, J., Zhou, T., Qu, Y., Bento, V. A., Qi, J., Xu, Y., Li, Y., & Wang, Q. (2023). An improved global vegetation health index dataset in detecting vegetation drought. *Scientific Data*, *10*(1). https://doi.org/10.1038/s41597-023-02255-3
46. Zhang, T., Zhou, Y., Zhu, Z., Li, X., & Asrar, G. R. (2021). *A global seamless 1 km resolution daily land surface temperature dataset (2003-2020)*. https://doi.org/10.25380/iastate.c.5078492